



Surplus charge injection enables high-cell-potential stable 2D polyaniline supercapacitors

Xinglin Jiang^a, Xiang Chu^a, Xiong Zhang^b, Yanting Xie^a, Tao Yang^a, Junfeng Huang^a, Wen Li^a, Weili Deng^a, Haitao Zhang^{a,*}, Weiqing Yang^a

^a Key Laboratory of Advanced Technologies of Materials, Ministry of Education, School of Materials Science and Engineering, Southwest Jiaotong University, Chengdu 610031, China

^b Institute of Electrical Engineering, Chinese Academy of Sciences, Beijing 100190, China

ARTICLE INFO

Keywords:

Surplus charge injection
2D polyaniline
Supercapacitors
High cell potential
Cycling stability
Energy density

ABSTRACT

The extraordinary pseudocapacitance of polyaniline (PANI) can be only realized in acid electrolytes with a limited potential window of 0.6~0.8 V. As the potential further increases, PANI will suffer from the hydrolysis issue, leading to molecular-chain fracture and oxidative failure. In this work, we propose a strategy of surplus electron injection to stabilize the molecular chain of PANI at high cell potential. The surplus electron injection in 2D PANI is realized by exceeding the stable potential induced by an asymmetric supercapacitor structure design. As excessive charges are poured, supramolecular hydrogen bonds presented at 2D PANI capture them and generate additional redox reaction, which suppresses the damage of 2D PANI molecular structure and simultaneously strengthens its capacitive behavior. This effect is vividly demonstrated by the modulated electronic structure as indicated by shifting up the Fermi level, shifting down the work function and increasing the electrical conductivity. Consequently, high cell potential (1.2 V) 2D PANI supercapacitors with sulfuric acid electrolyte deliver a much longer cycling lifetime (76.8% vs. 45.1% after 10,000 cycles) and a much higher energy density (19.9 vs. 7.53 Wh kg⁻¹) than that of low cell potential (0.8 V) 2D PANI counterpart. This work guides to a novel way to design high cell potential aqueous-solution supercapacitors.

1. Introduction

Supercapacitors (SCs) are promising candidates for future high-power devices due to their high-power density, fast charging/discharging, and long cycle life [1–4]. However, their low energy density (E) drawback (5–10 Wh kg⁻¹) greatly limits their broad applications [5, 6]. According to $E = 1/2CV^2$, the energy density of SCs can be increased by increasing specific capacitance (C) or by widening potential window (V). To be specific, widening V is a more efficient way because of its square relation with E . Meanwhile, higher V of SCs can reduce the necessity for much more connection as used in high-voltage output fields, such as electrical engineering and flexible electronics [7].

Aqueous supercapacitors have high ionic conductivity, high dielectric constant, small ionic size and facilitated faradaic capacitance because of using aqueous electrolytes [8]. However, the cell voltage of aqueous supercapacitors is limited by the thermodynamic decomposition voltage of water (1.23 V), which is almost within 1.0 V [9,10]. Thus, the successfully application of aqueous SCs critically relies on expanding

the electrochemical stability windows. For this purpose, some modification strategies from thermodynamics and dynamics have been widely reported to widen the potential window. On the thermodynamic side, the positive and negative electrodes with high difference in work function, such as MnO₂ and MoO₃ [11], can effectively broaden the potential window. Similarly, one electrochemical pre-charging strategy based on thermodynamic theory was used to boost the electrode potential by optimizing the zero potential charge (E_{0V}) [12]. On the kinetically side, the introduction of redox couples or the embeddedness of alkali metals on the electrode surface occupy the active sites of the electrode material to achieve higher potential window. This passivation effect inhibits the adsorption process at the electrode/electrolyte interface and the charge transfer process of H⁺/OH⁻ [13,14]. However, the strategy of broadening the potential window by adjusting E_{0V} strategy is not obvious, and non-negligible self-discharge phenomenon that hindering its development. In addition, shuttle of redox species deteriorates cyclic stability phenomenon and decreases the coulomb efficiency of the SCs.

It is a common sense that high specific capacitance of conjugated

* Corresponding author.

E-mail address: haitaozhang@swjtu.edu.cn (H. Zhang).

<https://doi.org/10.1016/j.electacta.2023.142052>

Received 22 August 2022; Received in revised form 10 January 2023; Accepted 13 February 2023

Available online 15 February 2023

0013-4686/© 2023 Elsevier Ltd. All rights reserved.

polymers like polyaniline (PANI) [1,15,16], polypyrrole (PPy) [17,18], poly [3,4-ethylenedioxythiophene] (PEDOT) [19], etc, can only be realized in aqueous electrolytes with a low work voltage of 0.6–0.8 V [20–22]. Once electrochemical potential window is further increased, they will suffer from severely additional problems including structural degradation, oxidation, or even collapse [23–26]. Naturally, polyaniline would transit into pernigraniline at fully oxidized state and further hydrolysis, leading to rapid degradation of electrochemical performance that is the primary reason to low potential window [20]. Therefore, it is fundamentally challenging yet technically critical to overcome the problematic molecular structure degradation at high-cell-potential and hence pave the way for high-cell-potential stable PANI SCs.

Herein we demonstrate a new principle of surplus charge injection to realize high-cell-potential stabilized 2D PANI supercapacitors. The excessive charges generated by high-cell-potential are injected into the 2D PANI. The injected charges would interact with dynamic hydrogen bond in 2D PANI, inducing an upward shift of the Fermi level and accordingly reduced work function. And the decline of work function leads to additional redox reactions that compensates for the capacitance loss. As a result, surplus charge injection enables an increment ratio of 50% in potential window, 19.9 Wh kg⁻¹ in energy density, and 44.9% suppressed decline in cycling stability.

2. Experimental section

2.1. Materials

Aniline, citric acid monohydrate, polyvinyl alcohol (PVA) with a polymerization degree of 1799 (analytical grade) and hydrochloric acid (36.5%, wt/wt in water) were purchased from Aladdin (Shanghai, China). Ammonium persulfate, sulfuric acid (98%, wt/wt in water) and potassium hydroxide (analytical grade) were purchased from Kelong Chemical Reagent Factory (Chengdu, China). Polyvinylidene fluoride (PVDF) was purchased from Aladdin (Shanghai, China). Polydimethylsiloxane (PDMS) was purchased from Dow Corning (USA). Polyethylene terephthalate (PET) sheets with a thickness of 100 μm were purchased from Lizhiyuan Plastic Factory (Dongguan, China). Sodium carboxymethyl cellulose (C₈H₁₁O₇Na) was purchased from DAICEL Corporation (Japan). Styrene-Butadiene Rubber (SBR) with solid content of 40% was purchased from Rion Corporation (Japan) and was used to enhance the viscosity of HPAC slurry for preparing compact electrode.

2.2. Preparation of 2D PANI inks

2D PANI Inks was synthesized from our previous work [27]. Under an ice bath, 3.1521 g (15 mmol) of citric acid monohydrate and 6.87 mL (75 mmol) of aniline were added to a mixed solution of 30 mL of deionized water and 6.75 mL of 6 M HCl. Separately, 4.29 g (18.75 mmol) of ammonium persulfate was dissolved in 15 mL of deionized water. The above two solutions were stirred evenly and left to stand for 20 min, then the solutions were mixed under stirring conditions, and reacted for 8 h under ice bath conditions to obtain PANI/CA hydrogel. Nanosheets are obtained by vacuum filtration to remove excess impurities. Finally, PANI/CA ink is obtained by dispersing the filter cake in deionized water.

2.3. Preparation of HPAC inks

HPAC was synthesized from our previous work (the BET SSA is approximately 3000 m² g⁻¹, single point adsorption total pore volume of pores at $P/P_0 = 0.99$ is 2.27 cm³ g⁻¹, micropore volumes is 0.55 cm³ g⁻¹) [28]. 15 g of KOH and 2.5 g of PVDF were firstly mixed, after grinding they were transferred into a nickel boat. With the protection of argon atmosphere (40 sccm), it was heated up to 380 °C at a rate of 4 °C min⁻¹ and then kept for 2 h. The rate was heated to 800 °C for 2 h. After natural

cooling to room temperature, the samples were removed and stirred with 2 M HCl for 12 h to remove the impurities. Finally, the hydrochloric acid was removed with deionized water and dried for 12 h to obtain HPAC powder. 0.2 g of HPAC powder was taken and ball-milled at 200 rpm for 30 min, then 5 mL of H₂O and 0.48 g of CMC–Na (1 wt%) were added and ball-milled at 400 rpm for 2 h. Finally, 10 mL of H₂O and 0.03 g of SBR were added and ball-milled at 300 rpm for 30 min. The slurry was filtered through a sieve and 20 mL of H₂O was added to obtain HPAC slurry.

2.4. Preparation of conventional PANI inks

Under an ice bath, 1095 μL of aniline and 2.7384 g of ammonium persulfate were added to 60 mL of 1 M HCl, respectively. The above two solutions were stirred evenly and left to stand for 20 min, then the solution was stirred for 8 h under ice bath conditions. Conventional PANI are obtained by vacuum filtration to remove excess impurities. Finally, conventional PANI ink is obtained by dispersing the filter cake in deionized water.

2.5. Fabrication of flexible supercapacitors

In a typical fabrication of PVA/H₂SO₄ gel electrolytes, 8 g of PVA and 8 g of H₂SO₄ were slowly added to 80 mL of deionized water. Then, the above solution was stirred in a water bath at 80 °C for about 1 h to form a clear and viscous solution.

Gold film was sputtered onto a commercial PET film with a thickness of 100 μm using a magnetron sputtering apparatus with a sputtering power of 40 W and sputtering time of 15 min. Then, the 2D PANI and HPAC slurries were sprayed onto the gold current collectors, respectively. After dropping the PVA/H₂SO₄ gel electrolyte in the middle of the positive and negative electrode, the whole device was encapsulated with PDMS to assemble into a flexible asymmetric supercapacitor. Two identical conventional polyaniline electrodes or 2D PANI electrodes are also assembled in the same way to form the corresponding symmetric supercapacitor.

When making the asymmetric supercapacitor, the mass matching will follow the equation:

$$\frac{m^+}{m^-} = \frac{C^- \Delta V^-}{C^+ \Delta V^+} \quad (1)$$

Where m is the mass of the electrode material, C is the specific capacitance, ΔV is the potential window. Therefore, in this ASC device system, 0.8 mg of 2D PANI on the gold film, as well as the mass of the HPAC negative material can be matched according to the optimal mass ratio between the electrodes $m^+/m^- = 0.93$.

2.6. Material characterization

The morphology of the samples was characterized using a JEOL JSM-7800 prime scanning electron microscope (SEM) with an accelerating voltage of 5–10 kV. Raman spectra were tested by an RM2000 micro confocal Raman spectrometer using a 514 nm laser beam. X-ray photoelectron spectroscopy (XPS) tests were performed on an ESCALAB 250Xi. Optical absorption properties were characterized by UV-Vis absorption spectroscopy (Techcomp UV2310II). A TENSOR II spectrometer (Bruker) was used to confirm the type of functional groups in the FTIR spectra. Orbital energies were determined by UPS (ESCALAB XI+) and for WF measurements, a bias of –5 V was applied to the sample and all with spectra were calibrated to the Fermi energy level when the binding energy measured on a clean metal surface was zero. Taking the electrolyte into consideration, both samples were immersed into electrolyte firstly and then the electrolyte was removed by thoroughly washed by hot water with a temperature of 80 °C. The only difference lies whether they are experienced surplus charge injection or not. Electron spin

resonance (ESR) spectra were obtained on a JES FA200 spectrometer.

2.7. Electrochemical properties characterization

The electrochemical properties of HPAC and 2D PANI inks were tested by CHI660E workstation (Chenhua, Shanghai, China) in a three-electrode configuration. 1 M H₂SO₄ was used as the electrolyte, mercurous sulfate and Pt foil were used as the reference and counter electrodes, respectively. Electrochemical characterizations of fabricated ASCs are carried out in two-electrode system with PVA/H₂SO₄ gel as the electrolyte. Cyclic voltammetry (CV), galvanostatic charge-discharge (GCD) and electrochemical impedance spectroscopy (EIS) technologies are carried out to evaluate the electrochemical properties. The CV curves were recorded at various scan rates ranging from 1 mV s⁻¹ to 2000 mV s⁻¹. GCD curves are tested with different current density from 0.5 to 40 A g⁻¹ (based on the total loading mass of electrochemical active materials). EIS was recorded in the frequency ranging from 100 kHz to 10 mHz. The cycling life test was conducted on an Arbin MSTAT4 multi-channel galvanostat/potentiostat instrument (Arbin, USA) using GCD techniques at a current density of 5 A g⁻¹.

The CV curve calculates the specific capacitance (C , F g⁻¹) with the following equation:

$$C = \frac{It}{m\Delta V} \quad (4)$$

Where I (A) is the discharge current, t (s) is the discharge time, m (g) is the mass of the active material, and ΔV (V) is the discharge voltage window.

The energy density (E , Wh kg⁻¹) and power density (P , kW kg⁻¹) of the assembled supercapacitor is calculated according to the following equation, respectively.

$$E = \frac{1}{2 \times 3.6} CV^2 \quad (5)$$

$$P = \frac{E}{t} \quad (6)$$

3. Results and discussion

Fig. 1a shows the cycling life of conventional PANI (c-PANI) based symmetrical supercapacitors with a potential window of 1.2 V. The specific capacitance only maintains 31.9% of the initial value, meaning very poor cycling stability. Actually, c-PANI materials with different morphologies, dimensions, and sizes were generally worked at a narrow potential window of 0.6~0.8 V [29,30]. It is a common sense that the molecular structure of c-PANI will suffer from breaking at higher voltage [21,31-33]. In fact, the work function of two electrode materials in SCs is directly related to the electrochemical stability window according to the following equations [13,34]:

$$E = E_0 + \Delta E_1 + \Delta E_2 \quad (7)$$

$$E = \frac{1}{F} (\omega^\beta - \omega^\alpha) N_A + \Delta E_1 + \Delta E_2 \quad (8)$$

Where E denotes the potential window, E_0 is the standard electrode potential, and E_1 and E_2 are the surface dipole potentials associated with the oxygen and hydrogen precipitation overpotentials at the positive and negative electrodes, respectively. The electrochemical potential difference between the positive and negative electrodes is given as $\omega^\beta - \omega^\alpha$, and N_A and F represent Avogadro's and Faraday's constants, respectively. The relationship between the two electrode materials and the electrochemical window of the device is shown in Fig. 1b. Hence, two electrodes with large work function difference can effectively broaden the electrochemical window.

Through supramolecular structure design to synthesize 2D PANI by polymerization of aniline monomer with citric acid, the hydrogen bonds originated from the amino groups in PANI and carboxyl groups in citric acid can interact with high-cell-potential injected charges to occur redox reactions shown in Fig. 1c, hydrogen bonds presented in 2D PANI are

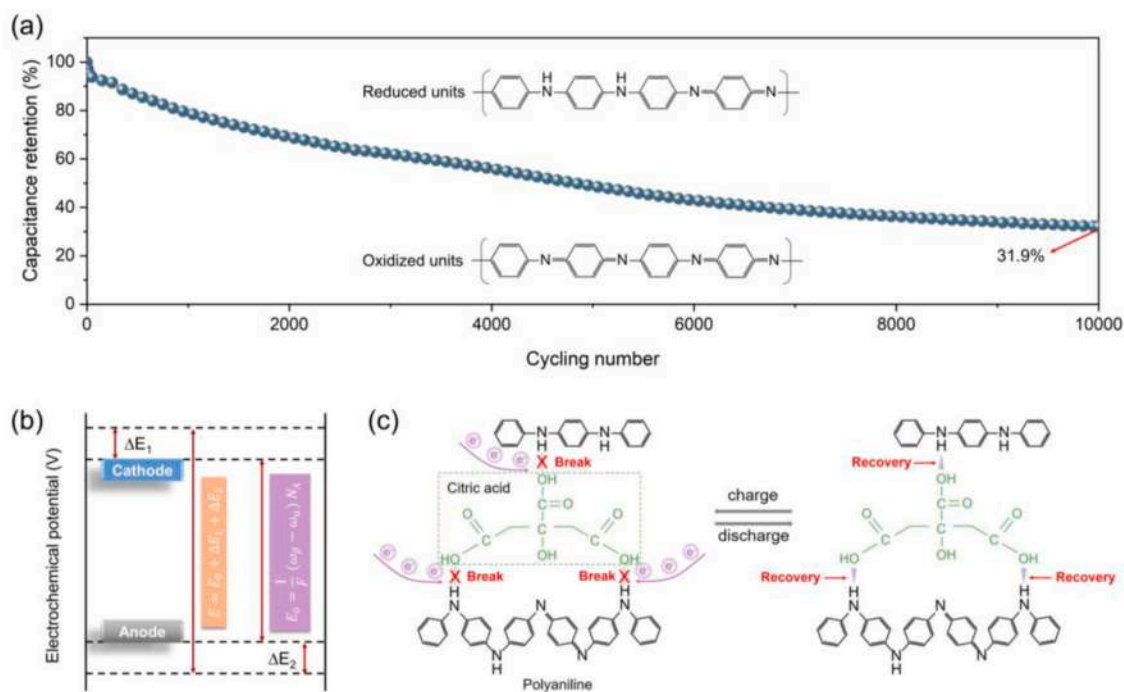


Fig. 1. Surplus charge injection unlocks rapid cycling degradation of two-dimensional polyaniline (2D-PANI) supercapacitors with high potential window. (a) The rapid capacitive degradation of conventional PANI (c-PANI) supercapacitors after 10,000 cycles. (b) Relationship between work function difference and the electrochemical window. (c) Dynamic hydrogen bonds in supramolecular 2D-PANI capture surplus injected charges and keep structural stability during repeated charging/discharging processes.

fractured during charging while recovered during discharging. Consequently, the molecular chains of PANI maintains integrity during the process of excess charge injection. More importantly, the removal of the overdoped citric acid leads to the upward shift of the Fermi level and band gap reduction of 2D PANI, which promotes the work function decrease and hence results in an enhanced electrochemical properties.

Since excessive charge injection is on basis of efficiently higher potential window while suppressing water hydrolysis, we constructed an asymmetrical structural design, where home-made hierarchically porous activated carbons (HPAC) and 2D PANI were used as the negative and positive electrodes, respectively. As shown in Fig. 2a, the capacity retention rates were 89.1%, 80.1%, and 76.8% after 10,000 cycles at 5 A g^{-1} as the potential windows were 0.8 V, 1.0 V and 1.2 V, respectively. The outstanding cycling stability at high operating voltage of 1.2 V is comparable or even exceeds some previously reported work on PANI-based SCs (Table S1) [35–42]. In addition, we also prove that surplus charge injection is efficient in symmetrical supercapacitors with 2D PANI materials as electrode materials. As shown in Fig. S1, with an electrochemical window of 0.8 V, the capacitance retention rates of symmetrical device 1 and device 2 were as low as 58.2% and 57.2% after 10,000 cycles at 5 A g^{-1} , which is a common value because of the poor electrochemical stability of conjugated polymers. Surprisingly, as the potential window increases to 1.2 V, the cycling stability is considerably increased to 85.8 and 84.5%. Meanwhile, EIS plots displayed in the inset of Fig. 2a were recorded for pristine and 10,000 cycled asymmetric supercapacitors (ASCs) with these three potential windows. Amazingly, the contact resistance (R_c) remains almost unchanged after 10,000 cycles at 1.0 and 1.2 V, implying that volume expansion induced molecular chain fracture is not severe. It should be noted that the R_c of 0.8 V cycled

devices becomes smaller after cycling, which is probably ascribed to the declined contact resistance between the electrolyte and 2D PANI electrode [43]. Definitely, charge transfer resistance (R_{ct}) is 0.2Ω at 1.0 V and remains unchanged after cycling, while changes from 0.3 to 0.7Ω at 1.2 V. The increased R_{ct} implies that the diffusion behavior of electrolyte ions in cycled 2D PANI is different from the pristine one, which we will discuss this variation later.

Firstly, we monitor the difference of electrode potential at different potential windows (Fig. 2b–d). Single electrode potential of HPAC and 2D PANI is illustrated in Fig. S2 and their maximum negative and positive potentials are -0.4 V and 0.6 V vs. $\text{Hg}/\text{Hg}_2\text{SO}_4$. As ASCs are charged to 0.8 V, the positive and negative electrodes are not exceeding the respective voltage limits. As the voltage increases to 1.0 V, the negative electrode potential is -0.47 V vs. $\text{Hg}/\text{Hg}_2\text{SO}_4$, exceeding the maximum negative potential of HPAC. As the voltage further increases to 1.2 V, the positive and negative electrode potentials are 0.64 V and -0.56 V vs. $\text{Hg}/\text{Hg}_2\text{SO}_4$, respectively, both exceeding their respective highest or lowest potentials, which guarantees the excessive charge injection into both negative and positive electrodes. Similarly, both the positive and negative electrodes of the symmetric 2D PANI-based supercapacitor are also injected with excessive charge at 1.2 V (Fig. S3).

The CV and GCD curves of the 2D PANI-based ASCs with the potential window of 0.8 V to 1.2 V are shown in Fig. 2e and 2f, respectively. The CV curve of the ASCs at 1.2 V shows double electrical layer (flat-top) and Faradaic (redox peak) storage characteristics, similar to the low potential window of 0.8 V. Interestingly, as the potential window is close to the water-splitting potential (1.23 V), there is no sign of electrolyte decomposition, unambiguously confirming the realization of high voltage window by asymmetrical structure design. Noted that the

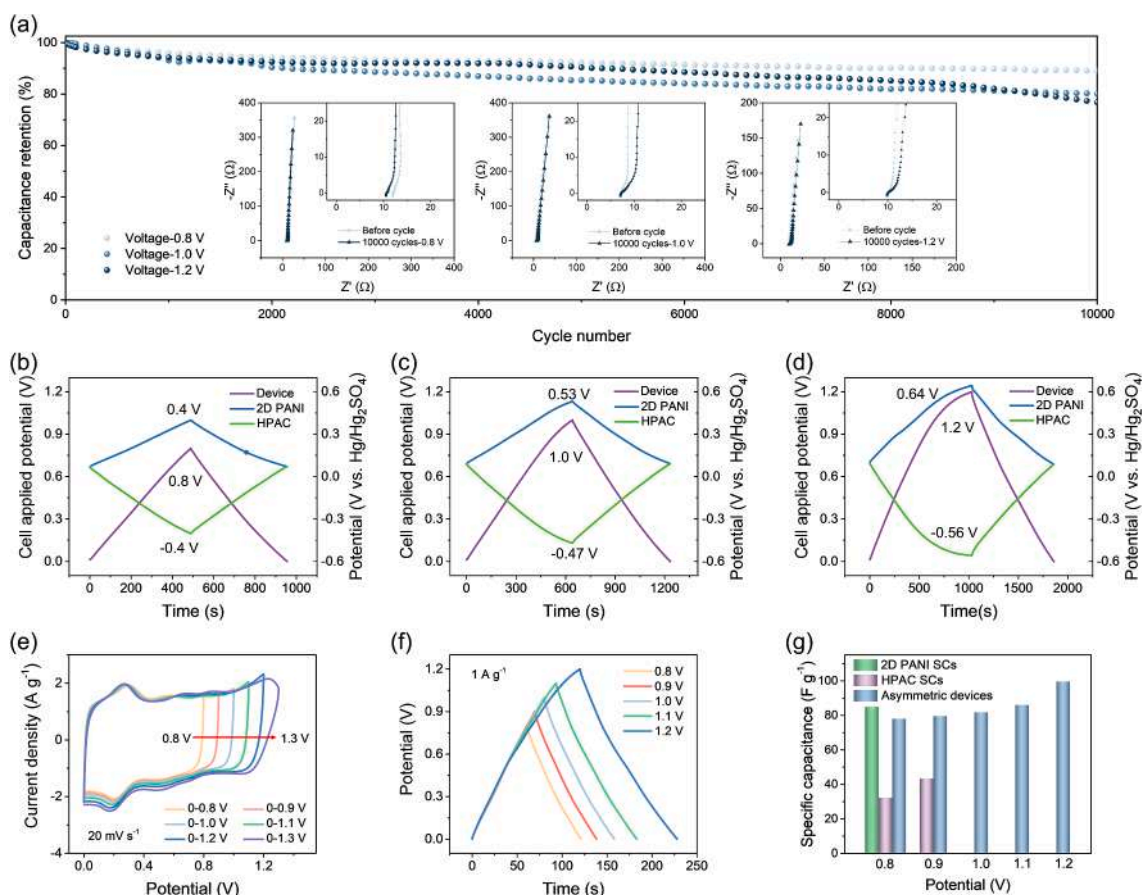


Fig. 2. High-voltage asymmetrical structure design. (a) Cycling stability at different potential windows. (b–d) The potential variation of the negative and positive electrode was charged/discharged at 1 mA cm^{-2} with different potential window of 0.8, 1.0, and 1.2 V. (e) CV curves of asymmetrical SCs at different potential windows. (f) GCD curves of asymmetrical SCs at a potential window up to 1.2 V. (g) The specific capacitance values at different potential windows.

deformation of CV curve at 1.3 V means the occurrence of hydrolysis. To understand the charge storage mechanism of the 2D PANI-based ASC, the current contributions of the surface control process and the diffusion control process are separated using the Dunn's method ($i = av^b$). Where a and b are constants, $b = 0.5$ indicates that the current is an electrochemical process controlled by diffusion, while $b = 1$ exhibits a charge storage mechanism similar to that of a capacitor [44]. As shown in Fig. S4a, the b -values corresponding to the anodic and cathodic peaks are 0.67 and 0.98, respectively, confirming that the charge storage mechanism in ASCs is a surface capacitance-dominated behavior, Fig. S4b is the capacitive part at 20 mV s⁻¹ and the detailed capacitive fraction plots are depicted in Fig. S4c, the capacity contribution of diffusion control decreases from 33.5% to 9.8% as the scan rate increases. At high scan rates, the redox reaction takes place at the electrode for a shorter period of time, resulting in sluggish reaction kinetics. The electrochemical properties of HPAC and 2D PANI symmetric counterparts were tested by CV, GCD, EIS (Figs. S5 and S6). At 0.5 A g⁻¹, ASCs possess a high specific capacitance of 99.5 F g⁻¹ on the basis of two electrodes at 1.2 V (398 F g⁻¹ for a single electrode), but it declines to 77.9, 79.5, 81.6, and 85.9 F g⁻¹ as the potential windows are 0.8–1.1 V (Fig. S7). The ASC also deliver higher in specific capacitance than that of HPAC (43.1 F g⁻¹) and 2D PANI (84.8 F g⁻¹) symmetrical counterparts (Fig. 2g). At 20 A g⁻¹, the capacitances of the ASCs are 67.2, 67.8, and 71.9 F g⁻¹ at 0.8, 1.0, 1.2 V, corresponding to 86.3%, 83.1%, and 72.3% retention of the capacitance at 0.5 A g⁻¹, respectively (Fig. S8 and Table S2).

Next, we examine the morphology, composition and structure evolution of the electrodes experienced surplus charge injection. As shown in Fig. S9, all the HPAC electrodes share similar carbon balls and hierarchically carbon bulks morphology, the degree of defects determined

by Raman spectra is 1.73, 1.71, 1.67, and 1.68 (Figs. S10–S13) [45]. On the other hand, as increasing voltage window, the content of epoxy-carbon bonds increases from 56.66% to 75.27%, while the content of carboxyl and hydroxyl carbon bonds decreased from 10.76% to 7.59% and 92.55% to 26.96%, respectively. The ratio of O/C content increased by 0.03 (Fig. S14). These results indicate that surplus charge injection causes slight oxidation of the anode material HPAC. Since the structural stability of carbon materials is much stronger than that of conjugated polymers, we will focus on the effect of surplus charge injection on the molecular chain and electronic structure of 2D PANI.

SEM images shown in Fig. 3a–d display that fresh 2D PANI has a loose and fluffy 2D platelets. After 10,000 durations at 0.8 V, the surface morphology remains similar. However, there are apparent secondary particles on the surface of 2D PANI as experiencing 10,000 cycles at 1.0 and 1.2 V and therefore highly rough surface. This secondary structure is usually considered to be a degradation product after the breakage of the polyaniline backbone following successive doping/de-doping of electrolytes and ions, which can block the redox active sites and lead to reduced capacitive performance and deteriorated cycling stability [46]. However, the excess charge injection did not severely impair the pseudocapacitance and cycling life of 2D PANI.

There is an apparent blue-shift phenomenon of two characteristic peaks of 2D PANI before and after charge injecting. One apparent responsive peak located at 1286 cm⁻¹ is assigned to the stretching vibrations of C–N in the polymer backbone [47]. The absorption peak of imine structure blue-shifts to 1292 cm⁻¹, 1293 cm⁻¹, 1295 cm⁻¹, respectively. A couple of characteristic absorption peaks at 1562 cm⁻¹ and 1487 cm⁻¹ in FTIR spectra correspond to the C=C stretching vibrations of quinone and benzene rings, respectively [48]. With the increase of the potential window, the absorption peak of the quinoid

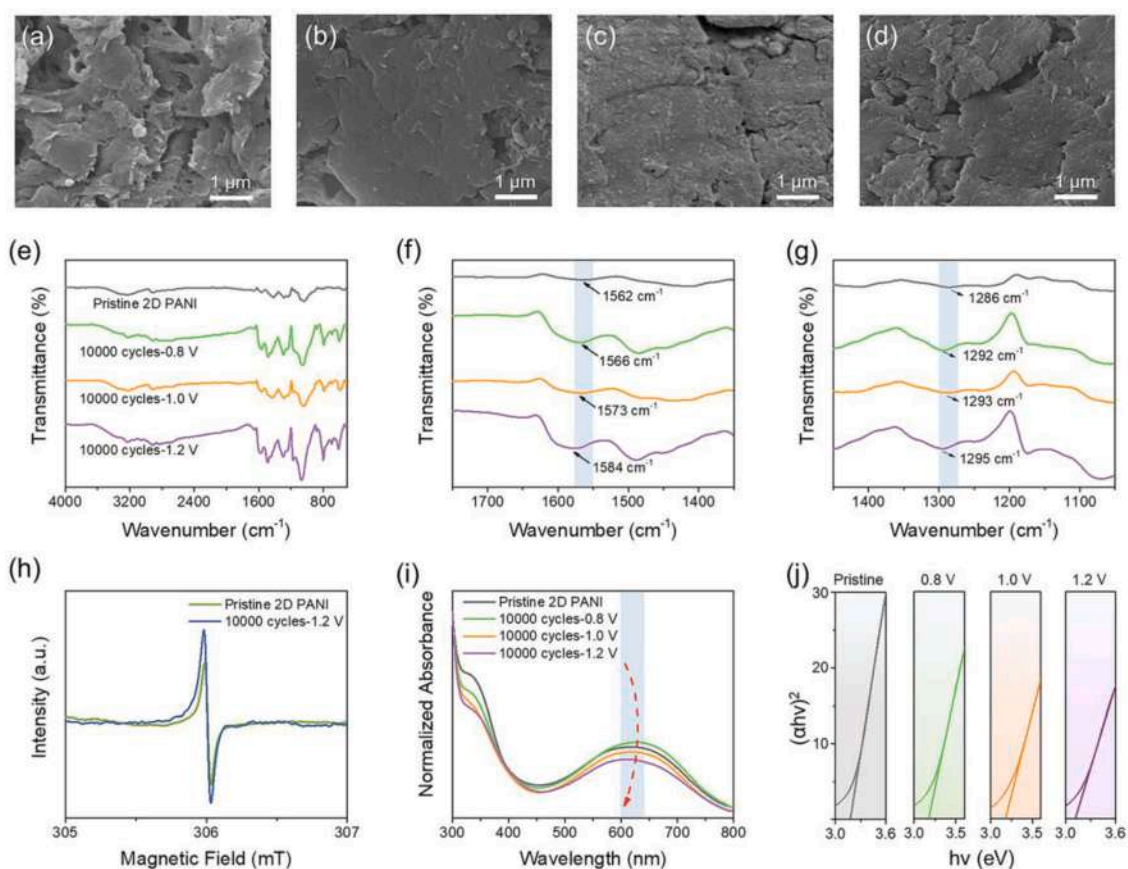


Fig. 3. Effect of surplus charge injection on the surface morphology, molecular structure, and optical absorbance for pristine and cycled 2D PANI. (a-d) SEM images of pristine 2D PANI (a), 0.8 V cycled 2D PANI (b), 1.0 V cycled 2D PANI (c), and 1.2 V cycled 2D PANI (d). (e) IR spectra. (f-g) The partially enlarged IR spectra. (h) ESR spectra. (i) UV-vis spectra. (j) Tauc's plot.

structure also blue-shifts to 1566 cm^{-1} , 1573 cm^{-1} , and 1581 cm^{-1} , respectively, meaning the broken of supramolecular hydrogen bonds. Higher potential window possesses more free charges. As they are injected into the molecular chain of 2D PANI, the electron withdrawing group of hydrogen bonds formed by amino and carboxyl groups will firstly capture them and occur the reduced reaction. As the charges separate from the molecular chain during discharging process, the loss of electrons induces the formation of hydrogen bonds again. Hence, the dynamic formation and fracture of supramolecular hydrogen bonds interact with excessive charges to stabilize the main molecular chain of 2D PANI. However, the coplanarity of the polyaniline molecular chain is broken and the conjugation length is reduced due to the enhanced steric hindrance effect by excessive charge injection, which causes the blue-shift of the characteristic peak of 2D PANI.

The electron spin-resonance spectroscopy (ESR) was further used to prove excessive charge injection induced declined coplanarity and shortened conjugation length. As shown in Fig. 3h, ESR spectra of 2D PANI before and after cycling share a single peak with equivalent g-factor of 2.213. However, the peak-to-peak linewidths of the ESR signals from pristine and cycled 2D PANI were 0.705 mT and 0.782 mT, respectively. After excess charge injection, the broadened width of linewidth of 2D PANI ascribes to a lower degree of electron delocalization that is originated from the reduced conjugation degree [49], which is consistent with the result of the blue shift of the characteristic peaks of FTIR.

To verify the increment of electrical conductivity by surplus charge injection, the UV-vis characterization is performed. As shown in Fig. 3i, the absorption peaks at 320 nm correspond to the $\pi\text{-}\pi^*$ transition of the benzene ring [50]. Another adsorption band at 618 nm is assigned to the charge-transfer excitons that are induced by the transition of the benzene-ring to adjacent quinone-ring structural PANI [51]. The characteristic peak of the imine structure was firstly red-shifted to 627 cm^{-1} , however, as the potential was increased to 1.2 V, the characteristic peak was blue-shifted to 617 cm^{-1} , which was attributed to the fact that excess charge injection reduces the conjugation length and destroys the coplanarity of the polyaniline molecular chains [52], which is consistent with the FTIR and ESR results. The optical band gap was calculated using the Tauc relation as following [53]:

$$\alpha h\nu = B(h\nu - E_g)^\gamma \quad (9)$$

Among them, α is the absorption coefficient, $h\nu$ is the photon energy, B is the band tail constant, E_g is the optical band gap, and γ is the value of the direct allowable transition, which is 1/2. By extrapolating the oblique line from the absorption peak, the value of its intersection with the abscissa $h\nu$ is E_g . As the operating voltage window increases, the E_g value decreases from 3.17 eV of pristine 2D PANI, to 3.15 eV of 0.8 V cycled 2D PANI, to 3.13 eV of 0.8 V cycled 2D PANI and further to 3.08 eV of 1.2 V cycled 2D PANI (Fig. 3j). This is probably due to high deficiency for pristine 2D PANI with cross-linked networks between PANI chains and citric acid molecules. After repeated charge/discharge at high voltage window, a part of citric acid is de-doped, which weakens

the protonation and improves the crystallinity of PANI, thereby higher conductivity, corresponding to smaller band gap [54,55].

To further determine the potential reason of this behavior, we collected the electronic structures of pristine and cycled 2D PANI were studied by ultraviolet photoelectron spectroscopy (UPS). As shown in Fig. 4a, the work function can be calculated by subtracting the secondary electron cutoff energy from the incident UV light source energy ($h\nu$) [56]. Since the energy of the incident UV source is 21.22 eV and the secondary electron cutoff energy of pristine 2D PANI is 17.45 eV, the work function of pristine 2D PANI is calculated as 3.77 eV. Similarly, the secondary cutoff energy of the 1.2 V cycled 2D PANI is 18.05 eV, and its work function is calculated to be $21.22 - 18.05\text{ eV} = 3.17\text{ eV}$, the energy difference between the Fermi level (E_F) and valence band maximum (E_{VBM}) of pristine 2D PANI and 1.2 V cycled 2D PANI is 1.6 eV and 2.0 eV, respectively.

The positions of E_F , E_{VBM} and vacuum level (E_{VAC}) before and after excess charge injection are shown in Fig. 4b, the energy difference between the Fermi energy level and the valence band top of 2D PANI increases by 0.4 eV and the work function decreases by 0.6 eV after excess charge injection. The Fermi energy levels of protonic acid-doped polyaniline are closely related to the degree of doping. Compared with the highly doped pristine 2D PANI, the removal of the overdoped citric acid in the 2D PANI after excess charge injection leads to a shift of the Fermi energy level away from the valence band, and this shift increases the crystallinity and contributes to the reduction of the 2D PANI work function [57]. To understand the potential window expansion, we plot a schematic of the relationship between the difference in work function of the SCs and the potential window (Fig. 4c). As reported, the internal potential difference of the device will be larger when the difference in work function is larger [58,59]. In this work, Excessive charge injection will reduce the work function of the positive material 2D PANI, resulting in an increase in the internal potential difference of the device, and 2D PANI can be stabilized in a higher potential window. In addition, it is known that the electron changes generated when polyaniline undergoes internal redox affect the work function. Therefore, this decrease in the work function may be due to the redox reaction that occurs when excessive charge is injected into the molecular chain of 2D PANI during the charging and discharging process and the hydrogen bonds are broken and then reduced.

Since the potential window is efficiently increased by 50%, the specific capacitance is greatly increased as verified by CV (Fig. 5a) and GCD (Fig. 5b) tests. And the corresponding energy and power density are also greatly improved (Table S2). Ragone plots shown in Fig. 5c give the energy density and power density of ASCs. The ASCs show a highest energy density of 19.9 Wh kg^{-1} with power density of 0.3 kW kg^{-1} , even with a high power density of 13.66 kW kg^{-1} , the energy density can still be maintained at 14.38 Wh kg^{-1} , indicating excellent rate performance. Thus, this work exceeds much of the previously reported work on PANI-based supercapacitors in terms of both energy density and power density [60–67].

To verify the integrability of the as-prepared ASCs, multiple

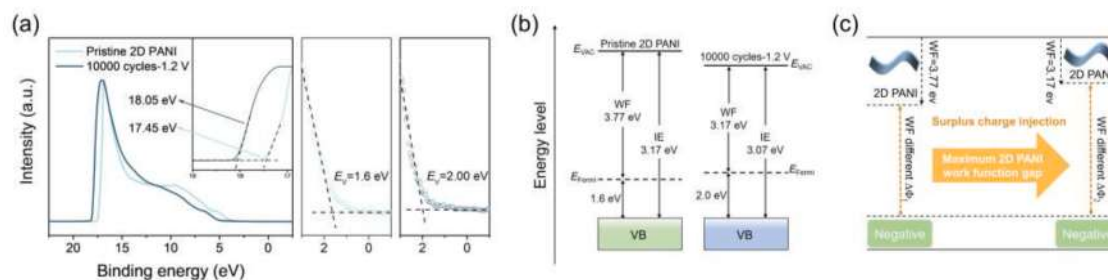


Fig. 4. Effect of surplus charge injection on electronic structure. (a) UPS spectra of pristine and cycled 2D PANI. Inset shows the secondary electron cut-off energy. The right panel shows the magnified view of the low binding energy region for E_{VBM} determination. (b) Schematic band energy diagram of pristine and cycled 2D PANI. (c) Schematically showing the widened potential window enabled by excess charge injection.

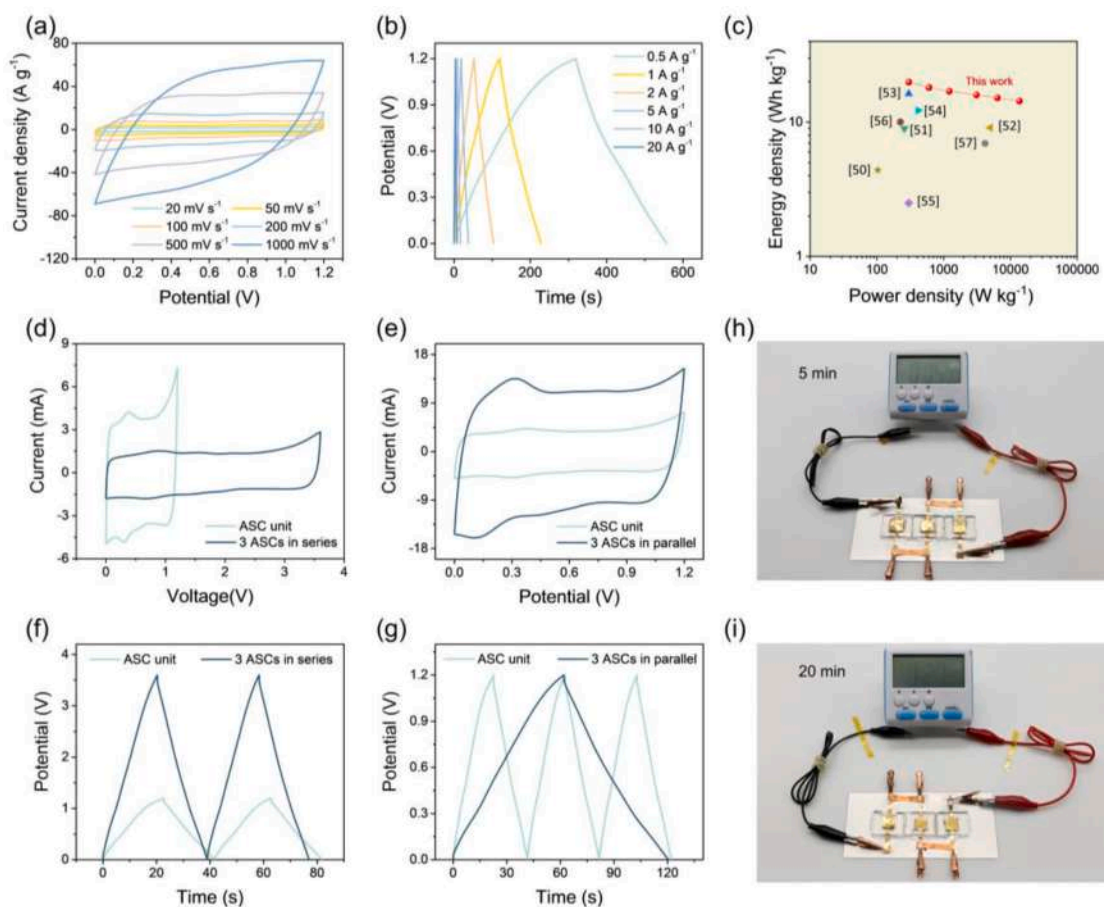


Fig. 5. Electrochemical performance of ASC. (a) CV curves of 2D PANI-based ASCs at different scan rates (from 20 to 1000 mV s^{-1}). (b) GCD curves of 2D PANI-based ASCs at different current densities (from 0.5 to 20 A g^{-1}). (c) Ragone plots of 2D PANI-based ASCs after excess charge injection and other state-of-the-art works. CV curves of ASCs connected in series (d) and in parallel (e). GCD curves of ASCs connected in series (f) and in parallel (g). (h-i) The recorded work time of 2D PANI-based symmetric supercapacitors and ASCs driving an LCD timer.

monolithic devices were connected in series or in parallel to achieve higher voltage or current output. Fig. 5d shows the CV curves of a single ASC device and three ASC devices in series. The working potential window can be expanded to 3.6 V (scanning rate is 20 mV s^{-1}) and the energy output is significantly improved. Fig. 5e shows the CV curves at 20 mV s^{-1} of a single ASC device and three ASCs devices in parallel. By paralleling, the output current is increased, thereby increasing the output capacitance. The series and parallel GCD curves show an enlargement of the working potential window and a prolongation of the discharge time, respectively (Fig. 5f,g). After cycling three symmetrical 2D PANI devices and three ASCs devices in series for 10,000 cycles, for lighting the LCD timer, the ASCs devices can sustain for 20 min while the symmetrical 2D PANI devices can only last for 5 min, unambiguously indicating the higher energy and longer cycling stability of ASCs (Fig. 5h, i). In addition, as a visual demonstration, ASCs devices can easily power up LED light signs and watches (Fig. S15).

4. Conclusion

In conclusion, surplus charge injection is an efficient strategy to enhance the potential window and simultaneously unlock the cycling instability of high-capacitive supercapacitor electrode materials. The excessive charge injection is realized by asymmetrical structure, in which HPAC was used as the negative electrode material and 2D PANI as the positive electrode material. With a long-term duration of surplus charge injection, the Fermi energy is increased by 0.4 eV, the work function is obviously decreased by 0.6 eV, and the optical band gaps are

changed from 3.17 to 3.07 eV. These electronic variations are related to the molecular chain and supramolecular hydrogen bonds, which is proved by the blue shift of C–N stretching vibration and the doped degree by proton hydrogen. Interestingly, the excessive charge injection leads to a high potential window of 1.2 V for 2D PANI supercapacitors with 1 M H_2SO_4 electrolyte, and accordingly higher energy density as well as longer cycling stability. This work provides an alternative way to solve the longstanding paradox between high potential window and large specific capacitance for supercapacitor electrode materials.

CRediT authorship contribution statement

Xinglin Jiang: Investigation, Methodology, Visualization, Writing – original draft. **Xiang Chu:** Visualization. **Xiong Zhang:** Formal analysis. **Yanting Xie:** Investigation, Methodology. **Tao Yang:** Investigation, Methodology. **Junfeng Huang:** Investigation, Methodology. **Wen Li:** Formal analysis. **Weili Deng:** Formal analysis. **Haitao Zhang:** Conceptualization, Formal analysis, Funding acquisition, Project administration, Supervision, Writing – review & editing. **Weiqing Yang:** Funding acquisition.

Declaration of Competing Interest

The authors declare that they have no known competing financial interests or personal relationships that could have appeared to influence the work reported in this paper.

Data availability

Data will be made available on request.

Acknowledgments

The acknowledgements come at the end of an article after the conclusions and before the notes and references. This work was supported by the National Natural Science Foundation of China (Nos. 51977185 and 51972277) and the Natural Science Foundation of Sichuan Province (No. 2023NSFC0441). We are thankful to the Analytical and Testing Center of Southwest Jiaotong University for providing the SEM measurements.

Supplementary materials

Supplementary material associated with this article can be found, in the online version, at [doi:10.1016/j.electacta.2023.142052](https://doi.org/10.1016/j.electacta.2023.142052).

References

- [1] P. Simon, Y. Gogotsi, Materials for electrochemical capacitors, *Nat. Mater.* 7 (2008) 845–854, <https://doi.org/10.1038/nmat2297>.
- [2] P. Simon, Y. Gogotsi, Perspectives for electrochemical capacitors and related devices, *Nat. Mater.* 19 (11) (2020) 1151–1163, <https://doi.org/10.1038/s41563-020-0747-z>.
- [3] Z. Wang, Z. Xu, H. Huang, X. Chu, Y. Xie, D. Xiong, C. Yan, H. Zhao, H. Zhang, W. Yang, Unraveling and regulating self-discharge behavior of $\text{Ti}_3\text{C}_2\text{T}_x$ MXene-based supercapacitors, *ACS Nano* 14 (2020) 4916–4924, <https://doi.org/10.1021/acsnano.0c01056>.
- [4] C. Li, X. Zhang, Z. Lv, K. Wang, X. Sun, X. Chen, Y. Ma, Scalable combustion synthesis of graphene-welded activated carbon for high-performance supercapacitors, *Chem. Eng. J.* 414 (2021), 128781, <https://doi.org/10.1016/j.cej.2021.128781>.
- [5] C. Choi, D.S. Ashby, D.M. Butts, R.H. DeBlock, Q. Wei, J. Lau, B. Dunn, Achieving high energy density and high power density with pseudocapacitive materials, *Nat. Rev. Mater.* 5 (2020) 5–19, <https://doi.org/10.1038/s41578-019-0142-z>.
- [6] Y. Xie, H. Zhang, H. Huang, Z. Wang, Z. Xu, H. Zhao, Y. Wang, N. Chen, W. Yang, High-voltage asymmetric MXene-based on-chip micro-supercapacitors, *Nano Energy* 74 (2020), 104928, <https://doi.org/10.1016/j.nanoen.2020.104928>.
- [7] Q. Wang, Y. Zhou, X. Zhao, K. Chen, B. Gu, T. Yang, H. Zhang, W. Yang, J. Chen, Tailoring carbon nanomaterials via a molecular scissor, *Nano Today* 36 (2021), 101033, <https://doi.org/10.1016/j.nantod.2020.101033>.
- [8] F. Beguin, V. Presser, A. Balducci, E. Frackowiak, Carbons and electrolytes for advanced supercapacitors, *Adv. Mater.* 26 (2014) 2219–2251, <https://doi.org/10.1002/adma.201304137>.
- [9] H. Wang, R. Tan, Z. Yang, Y. Feng, X. Duan, J. Ma, Stabilization perspective on metal anodes for aqueous batteries, *Adv. Energy Mater.* 11 (2021), <https://doi.org/10.1002/aenm.202000962>.
- [10] C. Zhong, Y. Deng, W. Hu, J. Qiao, L. Zhang, J. Zhang, A review of electrolyte materials and compositions for electrochemical supercapacitors, *Chem. Soc. Rev.* 44 (2015) 7484–7539, <https://doi.org/10.1039/c5cs00303b>.
- [11] J. Chang, M. Jin, F. Yao, T.H. Kim, L. Viet Thong, H. Yue, F. Gunes, B. Li, A. Ghosh, S. Xie, Y.H. Lee, Asymmetric supercapacitors based on graphene/ MnO_2 nanospheres and graphene/ MoO_3 nanosheets with high energy density, *Adv. Func. Mater.* 23 (2013) 5074–5083, <https://doi.org/10.1002/adfm.201301851>.
- [12] M. Yu, D. Lin, H. Feng, Y. Zeng, Y. Tong, X. Lu, Boosting the energy density of carbon-based aqueous supercapacitors by optimizing the surface charge, *Angew. Chem. Int. Ed.* 56 (2017) 5454–5459, <https://doi.org/10.1002/anie.201701737>.
- [13] R. Sahoo, P. Duy Tho, T.H. Lee, L. Thi Hoai Thuong, J. Seok, Y.H. Lee, Redox-driven route for widening voltage window in asymmetric supercapacitor, *ACS Nano* 12 (2018) 8494–8505, <https://doi.org/10.1021/acsnano.8b04040>.
- [14] T. Qin, H. Chen, Y. Zhang, X. Chen, L. Liu, D. Yan, S. Ma, J. Hou, F. Yu, S. Peng, Modulating surface chemistry of heteroatom-rich micropore carbon cloth electrode for aqueous 2.1V high-voltage window all-carbon supercapacitor, *J. Power Sources* 431 (2019) 232–238, <https://doi.org/10.1016/j.jpowsour.2019.05.004>.
- [15] Q. Zhang, E. Uchaker, S.L. Candelaria, G. Cao, Nanomaterials for energy conversion and storage, *Chem. Soc. Rev.* 42 (2013) 3127–3171, <https://doi.org/10.1039/c3cs00009e>.
- [16] X. Chu, X. Zhao, Y. Zhou, Y. Wang, X. Han, Y. Zhou, J. Ma, Z. Wang, H. Huang, Z. Xu, C. Yan, H. Zhang, W. Yang, J. Chen, An ultrathin robust polymer membrane for wearable solid-state electrochemical energy storage, *Nano Energy* 76 (2020), 105179, <https://doi.org/10.1016/j.nanoen.2020.105179>.
- [17] Y. Huang, H. Li, Z. Wang, M. Zhu, Z. Pei, Q. Xue, Y. Huang, C. Zhi, Nanostructured polypyrrole as a flexible electrode material of supercapacitor, *Nano Energy* 22 (2016) 422–438, <https://doi.org/10.1016/j.nanoen.2016.02.047>.
- [18] P. Naskar, A. Maiti, P. Chakraborty, D. Kundu, B. Biswas, A. Banerjee, Chemical supercapacitors: a review focusing on metallic compounds and conducting polymers, *J. Mater. Chem. A* 9 (2021) 1970–2017, <https://doi.org/10.1039/d0ta09655e>.
- [19] B. Anothumakkool, R. Soni, S.N. Bhange, S. Kurungot, Novel scalable synthesis of highly conducting and robust PEDOT paper for a high performance flexible solid supercapacitor, *Energy Environ. Sci.* 8 (2015) 1339–1347, <https://doi.org/10.1039/c5ee00142k>.
- [20] Q.e. Zhang, A.a. Zhou, J. Wang, J. Wu, H. Bai, Degradation-induced capacitance: a new insight into the superior capacitive performance of polyaniline/graphene composites, *Energy Environ. Sci.* 10 (2017) 2372–2382, <https://doi.org/10.1039/c7ee02018j>.
- [21] D.E. Stilwell, P. Su-Moon, Electrochemistry of conductive polymers. II. Electrochemical studies on growth properties of polyaniline, *J. Electrochem. Soc.* 135 (1988) 2254–2262, <https://doi.org/10.1149/1.2096248>.
- [22] K. Wang, X. Zhang, C. Li, X. Sun, Q. Meng, Y. Ma, Z. Wei, Chemically crosslinked hydrogel film leads to integrated flexible supercapacitors with superior performance, *Adv. Mater.* 27 (2015) 7451, <https://doi.org/10.1002/adma.201503543>.
- [23] P. Yu, Z. Zhang, L. Zheng, F. Teng, L. Hu, X. Fang, A novel sustainable flour derived hierarchical nitrogen-doped porous carbon/Polyaniline electrode for advanced asymmetric supercapacitors, *Adv. Energy Mater.* 6 (2016) 1601111, <https://doi.org/10.1002/aenm.201601111>.
- [24] H.-P. Cong, X.-C. Ren, P. Wang, S.-H. Yu, Flexible graphene-polyaniline composite paper for high-performance supercapacitor, *Energy Environ. Sci.* 6 (2013) 1185–1191, <https://doi.org/10.1039/c2ee24203f>.
- [25] H. Tang, J. Wang, H. Yin, H. Zhao, D. Wang, Z. Tang, Growth of polypyrrole ultrathin films on MoS_2 monolayers as high-performance supercapacitor electrodes, *Adv. Mater.* 27 (2015) 1117–1123, <https://doi.org/10.1002/adma.201404622>.
- [26] Y. Wang, X. Chu, Z. Zhu, D. Xiong, H. Zhang, W. Yang, Dynamically evolving 2D supramolecular polyaniline nanosheets for long-stability flexible supercapacitors, *Chem. Eng. J.* 423 (2021), 130203, <https://doi.org/10.1016/j.cej.2021.130203>.
- [27] X. Chu, G. Chen, X. Xiao, Z. Wang, T. Yang, Z. Xu, H. Huang, Y. Wang, C. Yan, N. Chen, H. Zhang, W. Yang, J. Chen, Air-stable conductive polymer ink for printed wearable micro-supercapacitors, *Small* 17 (2021), 2100956, <https://doi.org/10.1002/smll.202100956>.
- [28] H. Zhang, X. Zhang, Y. Ma, Enhanced capacitance supercapacitor electrodes from porous carbons with high mesoporous volume, *Electrochim. Acta* 184 (2015) 347–355, <https://doi.org/10.1016/j.electacta.2015.10.089>.
- [29] L.V. Lukachova, E.A. Shkerin, E.A. Puganova, E.E. Karyakina, S.G. Kiseleva, A. V. Orlov, G.P. Karpacheva, A.A. Karyakin, Electroactivity of chemically synthesized polyaniline in neutral and alkaline aqueous solutions - role of self-doping and external doping, *J. Electroanal. Chem.* 544 (2003) 59–63, [https://doi.org/10.1016/s0022-0728\(03\)00065-2](https://doi.org/10.1016/s0022-0728(03)00065-2).
- [30] L. Zhang, S.J. Dong, The electrocatalytic oxidation of ascorbic acid on polyaniline film synthesized in the presence of camphorsulfonic acid, *J. Electroanal. Chem.* 568 (2004) 189–194, <https://doi.org/10.1016/j.jelechem.2004.01.022>.
- [31] R. Mazeikiene, G. Niaura, A. Malinauskas, Raman spectroelectrochemical study on the kinetics of electrochemical degradation of polyaniline, *Polym. Degrad. Stab.* 93 (2008) 1742–1746, <https://doi.org/10.1016/j.polydegradstab.2008.07.028>.
- [32] H.N. Dinh, J.F. Ding, S.J. Xia, V.I. Birss, Multi-technique study of the anodic degradation of polyaniline films, *J. Electroanal. Chem.* 459 (1998) 45–56, [https://doi.org/10.1016/s0022-0728\(98\)00286-1](https://doi.org/10.1016/s0022-0728(98)00286-1).
- [33] J. Lopez-Palacios, E. Munoz, M. Aranzazu Heras, A. Colina, V. Ruiz, Study of polyaniline films degradation by thin-layer bidimensional spectroelectrochemistry, *Electrochim. Acta* 52 (2006) 234–239, <https://doi.org/10.1016/j.electacta.2006.04.061>.
- [34] N. Choudhary, C. Li, J. Moore, N. Nagaiah, L. Zhai, Y. Jung, J. Thomas, Asymmetric supercapacitor electrodes and devices, *Adv. Mater.* 29 (2017), 1605336, <https://doi.org/10.1002/adma.201605336>.
- [35] S. Cho, K.-H. Shin, J. Jang, Enhanced electrochemical performance of highly porous supercapacitor electrodes based on solution processed polyaniline thin films, *ACS Appl. Mater. Interfaces* 5 (2013) 9186–9193, <https://doi.org/10.1021/am402702y>.
- [36] A.K. Thakur, A.B. Deshmukh, R.B. Choudhary, I. Karbhal, M. Majumder, M. V. Shelke, Facile synthesis and electrochemical evaluation of PANI/CNT/ MoS_2 ternary composite as an electrode material for high performance supercapacitor, *Mater. Sci. Eng. B* 223 (2017) 24–34, <https://doi.org/10.1016/j.mseb.2017.05.001>.
- [37] J. Chao, J. Deng, W. Zhou, J. Liu, R. Hu, L. Yang, M. Zhu, O.G. Schmidt, Hierarchical nanoflowers assembled from MoS_2 /polyaniline sandwiched nanosheets for high-performance supercapacitors, *Electrochim. Acta* 243 (2017) 98–104, <https://doi.org/10.1016/j.electacta.2017.04.161>.
- [38] Y. Xi, G. Wei, X. Liu, M. Pang, L. Liu, Y. Yang, Y. Ji, V.Y. Izotov, N.I. Klyui, W. Han, Enhancing the cycling stability of the polyaniline hybrids benefited from the hollow manganese dioxide/acetylene black skeleton, *Chem. Eng. J.* 290 (2016) 361–370, <https://doi.org/10.1016/j.cej.2016.01.069>.
- [39] L. Wang, H. Yang, G. Pan, L. Miao, S. Chen, Y. Song, Polyaniline-carbon nanotubes@zeolite imidazolate framework67-carbon cloth hierarchical nanostructures for supercapacitor electrode, *Electrochim. Acta* 240 (2017) 16–23, <https://doi.org/10.1016/j.electacta.2017.04.035>.
- [40] Y. Zhu, H. Xu, P. Chen, Y. Bao, X. Jiang, Y. Chen, Electrochemical performance of polyaniline-coated gamma- MnO_2 on carbon cloth as flexible electrode for supercapacitor, *Electrochim. Acta* 413 (2022), 140146, <https://doi.org/10.1016/j.electacta.2022.140146>.

- [41] M. Dirican, M. Yanilmaz, A.M. Asiri, X. Zhang, Polyaniline/MnO₂/porous carbon nanofiber electrodes for supercapacitors, *J. Electroanal. Chem.* 861 (2020), 113995, <https://doi.org/10.1016/j.jelechem.2020.113995>.
- [42] F.S. Omar, A. Numan, N. Duraisamy, M.M. Ramly, K. Ramesh, S. Ramesh, Binary composite of polyaniline/copper cobaltite for high performance asymmetric supercapacitor application, *Electrochim. Acta* 227 (2017) 41–48, <https://doi.org/10.1016/j.electacta.2017.01.006>.
- [43] Q.T. Qu, B. Wang, L.C. Yang, Y. Shi, S. Tian, Y.P. Wu, Study on electrochemical performance of activated carbon in aqueous Li₂SO₄, Na₂SO₄ and K₂SO₄ electrolytes, *Electrochem. Commun.* 10 (2008) 1652–1655, <https://doi.org/10.1016/j.elecom.2008.08.020>.
- [44] T. Brezesinski, J. Wang, S.H. Tolbert, B. Dunn, Ordered mesoporous alpha-MoO₃ with iso-oriented nanocrystalline walls for thin-film pseudocapacitors, *Nat. Mater.* 9 (2010) 146–151, <https://doi.org/10.1038/nmat2612>.
- [45] B. Gu, H. Su, X. Chu, Q. Wang, H. Huang, J. He, T. Wu, W. Deng, H. Zhang, W. Yang, Rationally assembled porous carbon superstructures for advanced supercapacitors, *Chem. Eng. J.* 361 (2019) 1296–1303, <https://doi.org/10.1016/j.cej.2019.01.007>.
- [46] P. Zhang, X. Zhai, H. Huang, J. Zhou, X. Li, Y. He, Z. Guo, Capacitance fading mechanism and structural evolution of conductive polyaniline in electrochemical supercapacitor, *J. Mater. Sci. Electron.* 31 (2020) 14625–14634, <https://doi.org/10.1007/s10854-020-04025-y>.
- [47] X. Wang, D. Jiang, C. Jing, X. Liu, K. Li, M. Yu, S. Qi, Y. Zhang, Biotemplate Synthesis of Fe₃O₄/Polyaniline for Supercapacitor, *J. Energy Storage* 30 (2020), 101554, <https://doi.org/10.1016/j.est.2020.101554>.
- [48] X. He, Q. Liu, J. Liu, R. Li, H. Zhang, R. Chen, J. Wang, High-performance all-solid-state asymmetrical supercapacitors based on petal-like NiCo₂S₄/Polyaniline nanosheets, *Chem. Eng. J.* 325 (2017) 134–143, <https://doi.org/10.1016/j.cej.2017.05.043>.
- [49] J.E.P. da Silva, M.L.A. Temperini, S.I.C. de Torresi, Secondary doping of polyaniline studied by resonance Raman spectroscopy, *Electrochim. Acta* 44 (1999) 1887–1891, [https://doi.org/10.1016/S0013-4686\(98\)00330-2](https://doi.org/10.1016/S0013-4686(98)00330-2).
- [50] M. Hassan, K.R. Reddy, E. Haque, S.N. Faisal, S. Ghasemi, A.I. Minett, V.G. Gomes, Hierarchical assembly of graphene/polyaniline nanostructures to synthesize free-standing supercapacitor electrode, *Compos. Sci. Technol.* 98 (2014) 1–8, <https://doi.org/10.1016/j.compscitech.2014.04.007>.
- [51] I.D. Norris, M.M. Shaker, F.K. Ko, A.G. MacDiarmid, Electrostatic fabrication of ultrafine conducting fibers: polyaniline/polyethylene oxide blends, *Syn. Met.* 114 (2000) 109–114, [https://doi.org/10.1016/s0379-6779\(00\)00217-4](https://doi.org/10.1016/s0379-6779(00)00217-4).
- [52] W. Zheng, Y. Min, A.G. MacDiarmid, M. Angelopoulos, Y.H. Liao, A.J. Epstein, Aggregation and molecular conformation of doped polyaniline in chloroform solution, *Syn. Met.* 84 (1997) 109–110, [https://doi.org/10.1016/s0379-6779\(97\)80669-8](https://doi.org/10.1016/s0379-6779(97)80669-8).
- [53] S. Xiong, S.L. Phua, B.S. Dunn, J. Ma, X. Lu, Covalently bonded polyaniline-TiO₂ hybrids: a facile approach to highly stable anodic electrochromic materials with low oxidation potentials, *Chem. Mater.* 22 (2010) 255–260, <https://doi.org/10.1021/cm903058c>.
- [54] R.S. Biscaro, M.C. Rezende, R. Faez, Reactive doping of PANI-CSA and its use in microwave absorbing materials, *Polym. Adv. Technol.* 20 (2009) 28–34, <https://doi.org/10.1002/pat.1239>.
- [55] O. Abdulrazzaq, S.E. Bourdo, V. Saini, V.G. Bairi, E. Dervishi, T. Viswanathan, Z. A. Nima, A.S. Biris, Optimization of the protonation level of polyaniline-based hole-transport layers in bulk-heterojunction organic solar cells, *Energy Technol.* 1 (2013) 463–470, <https://doi.org/10.1002/ente.201300058>.
- [56] L. Zhang, Y. Li, X. Li, C. Li, R. Zhang, J.-J. Delaunay, H. Zhu, Solution-processed CuSbS₂ thin film: a promising earth-abundant photocathode for efficient visible-light-driven hydrogen evolution, *Nano Energy* 28 (2016) 135–142, <https://doi.org/10.1016/j.nanoen.2016.08.036>.
- [57] O. Abdulrazzaq, S.E. Bourdo, V. Saini, F. Watanabe, B. Barnes, A. Ghosh, A.S. Biris, Tuning the work function of polyaniline via camphorsulfonic acid: an X-ray photoelectron spectroscopy investigation, *RSC Adv.* 5 (2015) 33–40, <https://doi.org/10.1039/c4ra11832d>.
- [58] L. Peng, X. Wei, K. Song, H. Peng, L. Li, J. Hu, Y. Yang, H. Zhang, P. Xiao, The effect of work function difference between cathode and anode materials on the potential window of the supercapacitor, *Electrochim. Acta* 332 (2020), 135479, <https://doi.org/10.1016/j.electacta.2019.135479>.
- [59] K.S. Kumar, D. Pandey, J. Thomas, High voltage asymmetric supercapacitors developed by engineering electrode work functions, *ACS Energy Lett.* 6 (2021) 3590–3599, <https://doi.org/10.1021/acseenergylett.1c01484>.
- [60] F. Miao, C. Shao, X. Li, N. Lu, K. Wang, X. Zhang, Y. Liu, Polyaniline-coated electrospun carbon nanofibers with high mass loading and enhanced capacitive performance as freestanding electrodes for flexible solid-state supercapacitors, *Energy* 95 (2016) 233–241, <https://doi.org/10.1016/j.energy.2015.12.013>.
- [61] Y. Tan, Y. Liu, L. Kong, L. Kang, C. Xu, F. Ran, *In situ* doping of PANI nanocomposites by gold nanoparticles for high-performance electrochemical energy storage, *J. Appl. Polym. Sci.* 134 (2017) 45309, <https://doi.org/10.1002/app.45309>.
- [62] W. Xu, B. Mu, A. Wang, Morphology control of polyaniline by dopant grown on hollow carbon fibers as high-performance supercapacitor electrodes, *Cellulose* 24 (2017) 5579–5592, <https://doi.org/10.1007/s10570-017-1505-5>.
- [63] K. Jin, W. Zhang, Y. Wang, X. Guo, Z. Chen, L. Li, Y. Zhang, Z. Wang, J. Chen, L. Sun, T. Zhang, *In-situ* hybridization of polyaniline nanofibers on functionalized reduced graphene oxide films for high-performance supercapacitor, *Electrochim. Acta* 285 (2018) 221–229, <https://doi.org/10.1016/j.electacta.2018.07.220>.
- [64] C. Hu, X. Zhang, B. Liu, S. Chen, X. Liu, Y. Liu, J. Liu, J. Chen, Orderly and highly dense polyaniline nanorod arrays fenced on carbon nanofibers for all-solid-state flexible electrochemical energy storage, *Electrochim. Acta* 338 (2020), 135846, <https://doi.org/10.1016/j.electacta.2020.135846>.
- [65] H. Huang, S.C. Abbas, Q. Deng, Y. Ni, S. Cao, X. Ma, An all-paper, scalable and flexible supercapacitor based on vertically aligned polyaniline (PANI) nanodendrites@fibers, *J. Power Sources* 498 (2021), 229886, <https://doi.org/10.1016/j.jpowsour.2021.229886>.
- [66] X. Wang, D. Zhang, H. Zhang, L. Gong, Y. Yang, W. Zhao, S. Yu, Y. Yin, D. Sun, *In situ* polymerized polyaniline/MXene (V₂C) as building blocks of supercapacitor and ammonia sensor self-powered by electromagnetic-triboelectric hybrid generator, *Nano Energy* 88 (2021), 106242, <https://doi.org/10.1016/j.nanoen.2021.106242>.
- [67] H. Shen, H. Li, M. Li, C. Li, L. Qian, L. Su, B. Yang, High-performance aqueous symmetric supercapacitor based on polyaniline/vertical graphene/Ti multilayer electrodes, *Electrochim. Acta* 283 (2018) 410–418, <https://doi.org/10.1016/j.electacta.2018.06.182>.